nature immunology

A single class II myosin modulates T cell motility and stopping, but not synapse formation

Jordan Jacobelli[1], Stephen A Chmura[1], Denis B Buxton[2], Mark M Davis[3] & Matthew F Krummel[1]

Upon encountering an antigen, motile T cells stop crawling, change morphology and ultimately form an 'immunological synapse'. Although myosin motors are thought to mediate various aspects of this process, the molecules involved and their exact roles are not defined. Here we show that nonmuscle myosin heavy chain IIA, or MyH9, is the only class II myosin expressed in T cells and is associated with the uropod during crawling. MyH9 function is required for maintenance of the uropod and for T cell motility but is dispensable for synapse formation. Phosphorylation of MyH9 in its multimerization domain by T cell receptor–generated signals indicates that inactivation of this motor may be a key step in the 'stop' response during antigen recognition.

T lymphocytes circulate through vasculature into peripheral lymphoid tissues, scanning antigen-presenting cells (APCs) for peptide–major histocompatibility complex (MHC) ligands for their T cell receptors (TCRs). After leaving the vasculature, T cells acquire a polarized morphology and initiate crawling, probably as a result of chemotactic stimuli, earlier activating stimuli or both[1–3]. The characteristic 'hand-mirror' shape of a crawling T cell consists of a flattened leading edge followed by the nucleus and a handle-like tail termed the uropod[4]. Cells rapidly convert to a rounded morphology during peptide-MHC recognition and the ensuing formation of an immunological synapse[1,5,6].

Polarization during crawling is likely to be a mechanism for efficient motility as well as a response to chemotactic and adhesive stimuli. The leading edge of activated T cells is enriched with chemokine receptors such as CCR2 and CCR5 (ref. 7); it is also a site of integrin activation that permits pseudopodal projections to adhere to the surrounding substratum. The uropod, by contrast, contains the microtubule organizing center (MTOC) and the majority of cellular organelles and cytoplasmic volume. Current models indicate that integrins are deactivated at this site to allow retraction of the tail. However, it is also possible that various adhesion molecules at the uropod can tether cells and aid in extravasation[8].

For a T cell to stop crawling and convert to a rounded shape with a flattened surface at the synapse requires an encounter with an antigen-MHC–bearing APC[5,9]. After this early TCR triggering by agonist peptide-MHC complexes, T cells initiate the formation of an 'immature synapse' with the presenting APC. During this initial, highly dynamic phase, the TCR aggregates at the contact site as a series of microclusters, coinciding with the initiation of calcium signaling[10]. Over time, these microclusters coalesce into a characteristic mature synapse, defined by a central core of TCR-CD3 complexes surrounded by a ring of adhesion molecules[11,12]. The MTOC, formerly in the uropod, translocates to the contact site[13]. In this process, the nucleus is displaced away from the nascent synapse, the elongated projection that defines the uropod is lost and the T cell becomes more rounded[5]. In addition, a bulk surface movement seems to recruit membrane domains from the former uropod toward the APC, bringing with them membrane components that may reinforce signaling[14]. The changes in morphology and redistribution of receptors and lipid rafts that follow antigen recognition in T cells, and the speed at which these transitions occur, indicate that these events may be dependent on an intact cytoskeleton and are possibly motor driven[14–17].

Myosin motor proteins are likely candidates for mediating many of the events associated with synapse formation. Myosins are a superfamily of actin-based motor proteins consisting of approximately 40 members in 15 classes. These cellular motors have a variety of functions, including cytokinesis, migration, modulation of the retrograde flow of projections of the neural growth cone, influence on ruffling behavior, and possibly transport of cellular cargo along the actin cytoskeleton[18–20]. Myosins are able to generate ATP-dependent movement along actin filaments. Their structure consists of a globular head that can bind actin and has ATPase activity, a neck domain that binds myosin light chains or calmodulin, and a tail of variable length that can either promote multimerization or bind different cellular cargo. Although each family member has a unique C-terminal 'cargo' domain, the identity of the specific players involved in T cell responses remains obscure[18–20].

[1]Department of Pathology, University of California at San Francisco, 513 Parnassus Ave., San Francisco, California 93143, USA. [2]Laboratory of Molecular Cardiology, National Heart, Lung and Blood Institute, National Institutes of Health, Bethesda, Maryland 20892, USA. [3]Department of Microbiology and Immunology, Stanford University School of Medicine and the Howard Hughes Medical Institute, Stanford, California 94305, USA. Correspondence should be addressed to M.F.K. (krummel@itsa.ucsf.edu).

Published online 4 April 2004; doi:10.1038/ni1065

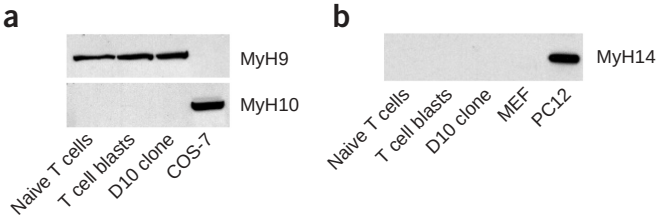

Figure 1 MyH9 is the predominant class II myosin motor expressed in T cells. (**a**) Immunoblot analysis of cell lysates from naive DO11.10 CD4$^+$ T cells, day 6 DO11.10 activated T cells, D10 T cell clones or COS-7 cells with MyH9 (upper) or MyH10 (lower) isoform-specific antibodies. (**b**) Immunoblot analysis of cell lysates from naive DO11.10 CD4$^+$ T cells, day 6 DO11.10 activated T cells, D10 T cell clones or MEF cells (as a negative control) and PC12 (as a positive control) with MyH14 isoform specific-antibodies. Similar amounts of lysates were loaded in each gel, as determined by protein assay. Results shown are representative of three (**a**) and two (**b**) independent experiments.

A subclass of myosin motors, the class II myosins, have been proposed to have a crucial role in regulating polarity and synapse formation, in part because their orthologs in the amoeba *Dictyostelium discoideum* are required for receptor capping. The class II nonmuscle myosin family consists of two widely expressed isoforms, myosin-IIA and myosin-IIB[19], and a third, less-characterized isoform, myosin-IIC, that was recently identified by genome sequencing and is expressed mainly in the intestine, colon and skeletal muscle[20,21]. Class II myosins are heterohexamers composed of two heavy chains and two pairs of light chains. Myosin-II molecules further self-assemble into bipolar multimeric filaments through interaction of their α-helical coiled-coil domains in the tail region. These myosin filaments can cross-link and contract actin filaments and provide tension to the cell. Their formation is necessary for many cellular functions, such as the separation of daughter cells during cytokinesis[22,23]. Class II myosins are also important in *D. discoideum* migration[24,25].

To assess the function of class II myosins in T cell crawling and synapse formation, we have extensively analyzed the expression patterns of these molecules in mouse T cells. Nonmuscle myosin heavy chain IIA (NMMHC-IIA, MyH9) was the sole class II myosin expressed in T cells and was highly enriched in the uropod. Whereas clusters of MyH9 seemed to move away from pseudopodia and toward the uropod during crawling, the protein ultimately translocated to the synapse after TCR ligation. However, inhibition of MyH9 disrupted uropod formation and crawling but not mature synapse formation. The change in localization of MyH9 seemed to be directly linked to TCR triggering, as the tail domain was phosphorylated after peptide-MHC or anti-CD3 stimulation and this phosphorylation was mediated directly by a rise in intracellular calcium. We suggest that this phosphorylation event represents a means by which the detection of antigen by T cells may inhibit motility of the cell by inactivating MyH9.

RESULTS

T cell expression of class II myosin motors

Because earlier evidence has indicated that myosin motors could control T cell morphology and receptor reorientation during crawling and synapse formation, we screened mouse T cell–derived cDNA for myosin family members using a degenerate PCR approach. Among the myosins that our screening identified as being highly expressed in T cells was the class II nonmuscle heavy chain myosin MyH9. To determine class II myosin heavy chain expression in T cells, we assessed protein expression in lysates from freshly isolated CD4$^+$ T cells, day 6 activated T lymphocytes, a conalbumin-specific CD4$^+$ T cell clone D10.G4-IL2 (D10) and control cells. We readily detected MyH9 protein in all T cells, but did not detect either MyH10 (NMMHC-IIB) or MyH14 (NMMHC-IIC; **Fig. 1**). Semiquantitative PCR analysis also did not detect MyH10 or MyH14 mRNAs in naive T cells or the D10 clone (data not shown).

To analyze the distribution of MyH9 in T cells during crawling and synapse formation, we generated stable transfectants of D10 T cell clones expressing a previously described fusion protein of human MyH9 with the green fluorescent protein (MyH9-GFP)[26]. These cells were analyzed by time-lapse fluorescence microscopy. During crawling,

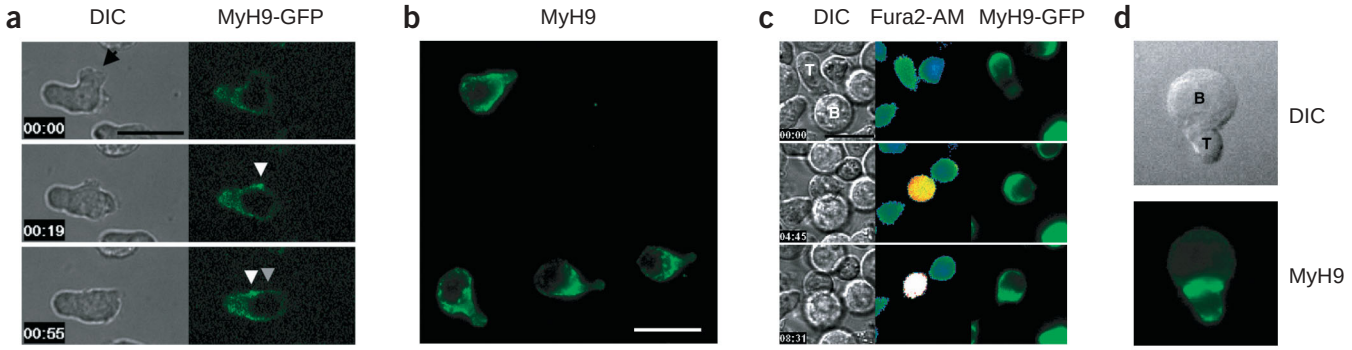

Figure 2 MyH9 is enriched and recycled at the uropod of crawling T cells and repolarizes to the T cell–APC interface during synapse formation. (**a**) Localization of MyH9-GFP in crawling lymphocytes. Individual time points from top to bottom (also see **Supplementary Video 1**) showing DIC (left) and fluorescence (right) of an MyH9-GFP transfected D10 T cell clone crawling from left to right within field. Black arrow marks the initial protrusion site of a pseudopod; white and gray arrows follow the localization of MyH9-GFP enriched packets over time (min:s). (**b**) Representative image of MyH9 distribution in crawling D10 T cells. Cells were seeded on glass coverslips, incubated for 30 min at 37 °C and then fixed, permeabilized and stained with anti-MyH9. (**c**) Timing of MyH9 polarization to the synapse. Shown, for individual time points, are simultaneous DIC (left), calcium concentration (as measured by Fura2-AM displayed in pseudo-color scale; middle), and MyH9-GFP fluorescence (right) images of transfected D10 T cell clones during coupling with antigen-pulsed APCs (also see **Supplementary Video 2**). Time 00:00 is arbitrarily set at the initial contact between T cell and APC. (**d**) MyH9 polarization to the synapse. T cells and antigen-pulsed B cells were mixed together and incubated for 30 min at 37 °C; the conjugates were fixed in paraformaldehyde and spotted on glass coverslips. The cells were then permeabilized and stained with anti-MyH9. DIC and fluorescence images are shown for a representative T cell–APC conjugate. Bars, 10 μm. Similar results were obtained in three independent experiments.

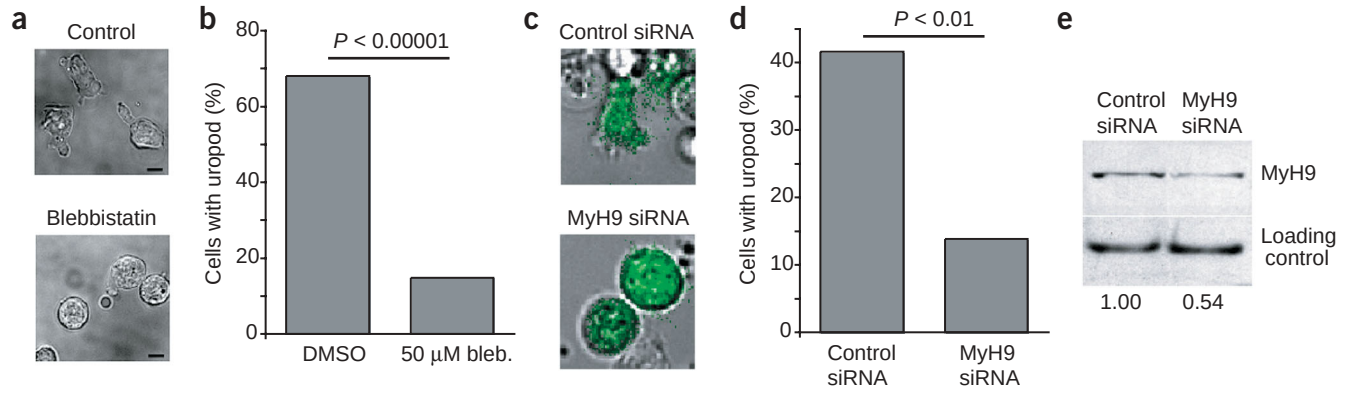

Figure 3 MyH9 motor activity is required for T cell polarity. (**a**) DIC images of D10 T cells treated with vehicle control (DMSO) or 50 μM blebbistatin. (**b**) Quantification of the loss of uropodal morphology of blebbistatin-treated cells ($n = 50$). (**c**) siRNA downregulation of MyH9 expression induces loss of uropod projections in T cells. Overlay of DIC and green fluorescence images showing morphology and GFP positivity of control and siRNA transfected D10 T cells. (**d**) Quantification of the loss of uropod projections by anti-MyH9 siRNA treatment ($n = 36$). (**e**) Immunoblot and densitometry data (shown as normalized protein abundance relative to control) for downregulation of MyH9 protein expression by siRNA. Similar results were obtained in three independent experiments.

MyH9 was not uniformly expressed throughout the cell but was instead enriched in the uropod (**Fig. 2a**). We confirmed the general distribution of endogenous MyH9 protein in fixed, nontransfected cells using MyH9-specific antibodies (**Fig. 2b**). Time-lapse analysis also showed higher-density packets of this motor protein at the sites where pseudopodal projections were reabsorbed and at the head-tail junction. Although they were indistinguishable by other means, these packets showed two distinct behaviors with respect to cellular positioning. One type of MyH9 packet stayed in approximately the same position along the cell border, whereas a second type recycled toward the uropod with an average normalized speed of 0.21 ± 0.04 μm/s relative to the cell body (eight packets analyzed from five different cells; **Fig. 2a** and **Supplementary Video 1**).

We then characterized the bulk distribution of MyH9 during T cell–APC conjugation and immunological synapse formation. After the encounter with antigen-pulsed APCs, most MyH9-GFP rapidly relocalized from the rear to the front of a motile cell, typically within minutes after the onset of calcium signaling and coincident with the transition from hand-mirror to round shape (**Fig. 2c** and **Supplementary Video 2**; quantified in **Supplementary Fig. 1**). In addition, this translocation was coordinated with the rearward movement of the nucleus, indicating that the relocalization of MyH9 could be tied to the general cytoplasmic repolarization process. We confirmed that endogenous MyH9 was localized at the synapse in fixed, untransfected T cell blast–APC couples using isoform-specific MyH9 antibodies (**Fig. 2d**). Thus, our data show that MyH9 is the only class II myosin expressed in T cells and that it is enriched at the uropod in crawling T cells but redistributes to the T cell–APC interface upon formation of the immunological synapse.

MyH9 regulation of T cell morphology and motility

Although the uropodal distribution during crawling implied a possible role for MyH9 in mediating motility, synapse localization also indicated that it might function during receptor recruitment and signaling. To establish the role of MyH9 in promoting these two processes, we assessed whether inhibition of MyH9 would affect either T cell crawling and the formation, or maintenance, of an ameboid morphology or the formation of the immunological synapse. For these studies we used the chemical inhibitor blebbistatin, which is a highly specific inhibitor of class II myosin ATPase activity[23].

Treatment of D10 T cells with 50 μM blebbistatin resulted in cell rounding and the disappearance of the uropod (**Fig. 3a**). We quantified this effect by measuring the percentage of T cells treated with blebbistatin or with dimethyl sulfoxide (DMSO), as a vehicle control, that had a uropodal morphology. Cells treated with the inhibitor were significantly less polarized: only 14.8% had a uropod as compared to 68% of control cells ($P < 0.00001$, **Fig. 3b**). We also measured the loss of uropodal morphology by calculating the elliptical form factor of

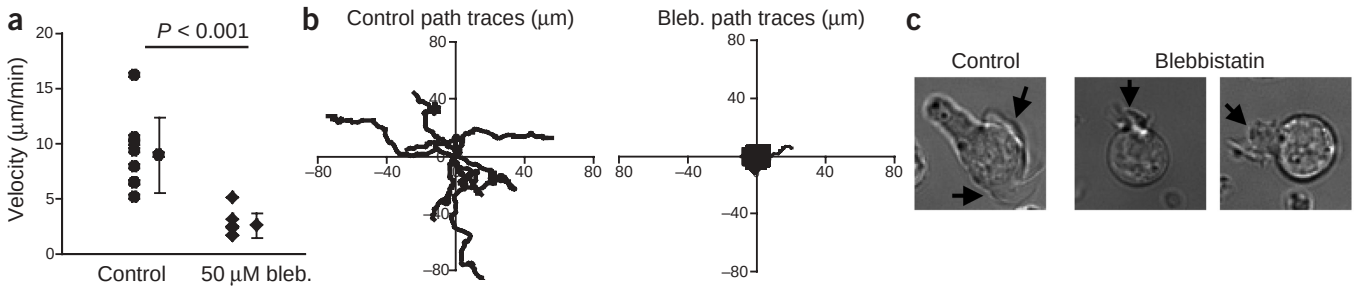

Figure 4 MyH9 function is necessary for T cell crawling. (**a**) Quantification of the effect of blebbistatin on crawling velocities of T cells, showing velocities of single cells and average values ($n = 8$). (**b**) Migration paths of D10 T cells treated with vehicle control or 50 μM blebbistatin. (**c**) DIC images of vehicle or blebbistatin-treated cells showing active formation of pseudopodal protrusions (black arrows). Results shown are representative of three independent experiments.

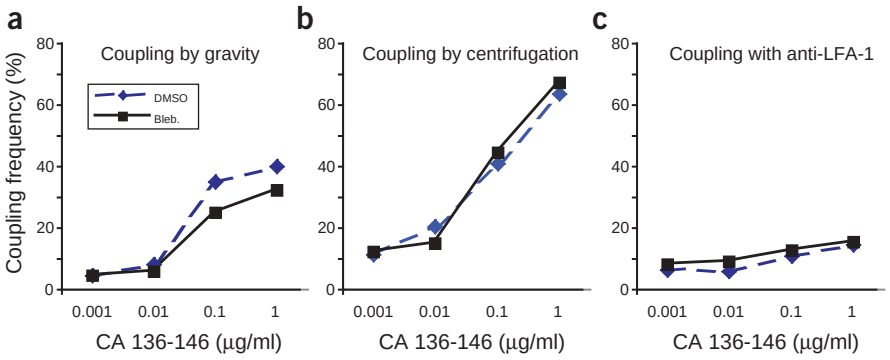

Figure 5 Pharmacological inhibition of MyH9 does not prevent T cell-B cell coupling. CFSE-labeled D10 T cells treated with 50 μM blebbistatin or vehicle control (DMSO) were allowed to couple with PKH-labeled APCs for 45 min at 37 °C and then analyzed by cytofluorimetry. T cells forming conjugates with B cells were quantified as a percentage of all T cells in the sample. (**a**) T and B cells were allowed to couple without centrifugation. (**b**) T and B cells were coupled by a brief initial spinning. (**c**) Coupling formation in the presence of blocking antibodies to LFA-1. Graphs are representative of one of three independent experiments. The amount of conalbumin peptide-loading of B cells is indicated on the x axis.

the cells (see Methods) and, although we observed a broad shape distribution, these results confirmed that blebbistatin-treated T cells were significantly less elongated than control cells ($P < 0.001$; **Supplementary Fig. 2**). To confirm the results obtained with blebbistatin and to further assess the specificity of MyH9 in regulating T cell morphology, we used an siRNA approach to block MyH9 protein expression. We observed a similar loss of polarization for siRNA-transfected D10 T cells (**Fig. 3c**,**d**), although inhibition of MyH9 expression was not complete (**Fig. 3e**). Because of the partial effect of siRNA inhibition of MyH9 expression and the low cell recovery, we limited our use of this approach to cell polarity experiments.

Next, we measured the effects of MyH9 blockade on crawling through analyses of center-of-mass velocity and path length. D10 T cells treated with blebbistatin were essentially nonmotile, whereas untreated cells crawled at about 9 μm/min, similar to speeds observed *in vivo*[2] (**Fig. 4a**,**b**). Live imaging of D10 T cells in which MyH9 activity was blocked showed that these cells were not completely inactive, as they could still generate pseudopods similar to those observed at the leading edge of untreated cells (**Fig. 4c**). Pseudopod formation was never followed by cellular translocation in blebbistatin-treated cells (**Fig. 4a**,**b**). Thus, class II myosin motor function in T cells is required for their characteristic ameboid uropodal morphology as well as their migratory capacity.

MyH9 is not required for synapse formation

The observation that a motor protein was required for a uropodal phenotype and for cellular translocation did not preclude its functioning during synapse formation. We therefore analyzed synapse formation while inhibiting MyH9 motor function. We initially used a cytofluorimetry–based conjugation assay. Carboxyfluorescein diacetate succinimidyl ester (CFSE)-loaded D10 T cells were pretreated with 50 μM blebbistatin or DMSO as the vehicle control and then mixed with conalbumin peptide–bearing APCs labeled with the red fluorescent dye PKH26. After a 45-min incubation, the cells were analyzed by flow cytometry for the presence of conjugates. Subtle differences in cell conjugation efficiency between blebbistatin-treated and control T cells were observed when the assay was performed by mixing together T cells and APCs in flat-bottom dishes at low densities without centrifugation (**Fig. 5a**). This result was most likely dependent on the motility defect of blebbistatin-treated T cells.

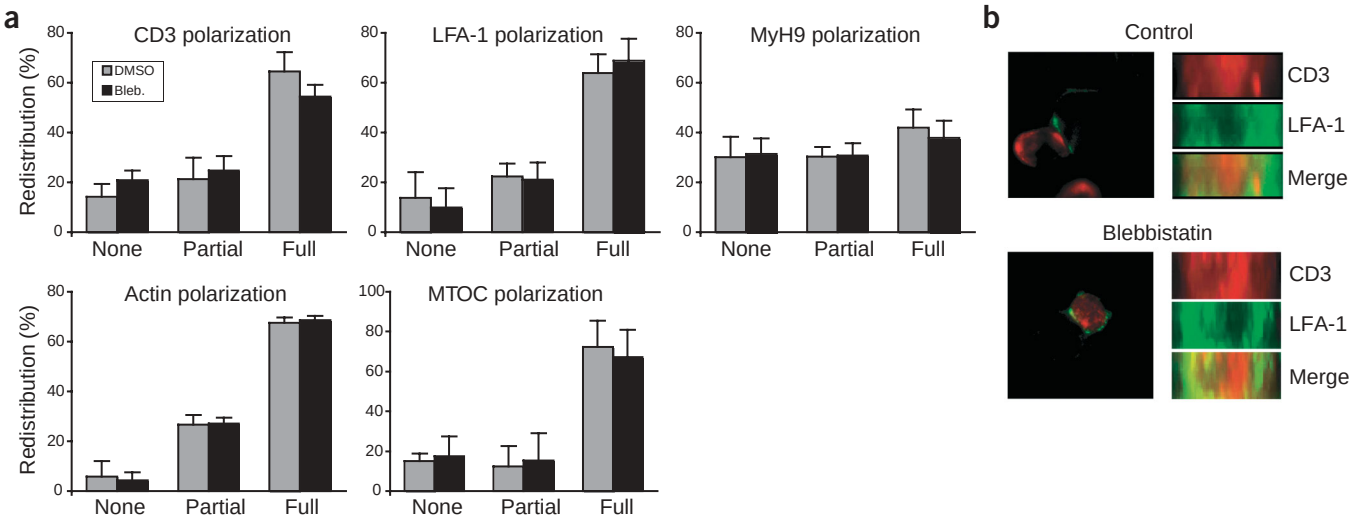

Figure 6 MyH9 inhibition does not prevent relocalization of immunological synapse and cytoskeletal components. (**a**) T cells treated with vehicle control (DMSO) or 50 μM blebbistatin were spun together with antigen-pulsed B cells, incubated 30 min at 37 °C and then fixed and plated on slides. Cells were permeabilized and stained for CD3, LFA-1, MyH9, actin and tubulin. T cell–APC conjugates were then scored for polarization and the relative redistribution percentages from three independent experiments were averaged and graphed. (**b**) CD3 and LFA-1 three-dimensional SMAC formation in cells treated with DMSO or blebbistatin. Left, color-combined maximal projection image of the Z-stacks with CD3 in red and LFA-1 in green; right, reconstructed front view of the interface. Results shown are representative of three independent experiments.

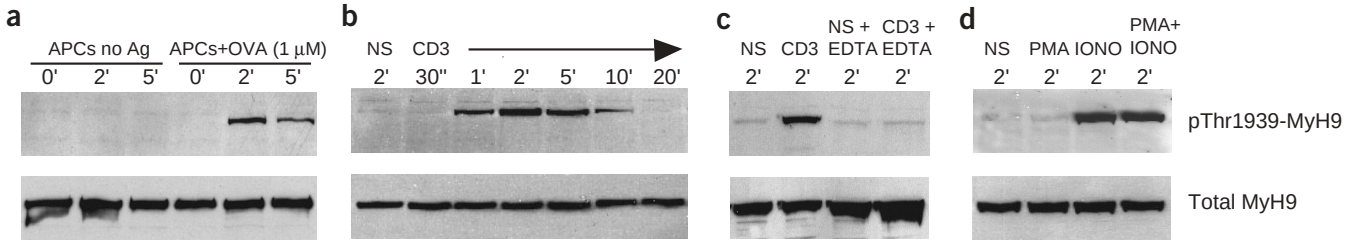

Figure 7 MyH9 is phosphorylated at threonine residues in response to TCR recognition. (**a**) DO11.10 T cell blasts were mixed 2:1 with APCs pulsed with antigen, or unpulsed control APCs, and incubated at 37 °C for the indicated times (', minutes; ", seconds). Cell lysates were then analyzed by immunoblotting with a phosphorylation state–specific anti-pThr1939-MyH9 and subsequently stripped and reblotted with an anti-MyH9. (**b**) DO11.10 T cell blasts were left untreated (NS) or incubated with anti-CD3 for 30 min at 4 °C and cross-linked with soluble goat anti-hamster for the indicated times at 37 °C. Cell lysates were then analyzed as in **a**. (**c**) DO11.10 T cell blasts were left untreated (NS) or incubated with anti-CD3 and then cross-linked as in **b** for 2 min. The entire stimulation procedure was carried out in PBS with calcium and magnesium or in PBS without calcium and magnesium and with 5 mM EDTA added (+EDTA). Cell lysates were analyzed as in **a**. (**d**) DO11.10 T cell blasts were left untreated (NS) or stimulated for 2 min with PMA, ionomycin or both. Cell lysates were analyzed as in **a**. Results are representative of three independent experiments.

In contrast, no difference in conjugation frequency was detected when cells were spun together at higher densities to bypass the need for crawling by the T cells. Therefore, even with blebbistatin inhibition, T cells were completely competent to form antigen-dependent adhesive contacts (**Fig. 5b**). Sampling at various times after centrifugation did not show any kinetic differences in cell conjugation efficiency, even as early as 1 min after incubation (data not shown). Blockade of interactions between the adhesion molecules LFA-1 and ICAM-1 reliably inhibited conjugate formation in the presence or absence of blebbistatin, showing that integrin function was responsible for this effect even in the absence of MyH9 activity (**Fig. 5c**).

Although these results indicated that MyH9 activity was not required for the formation of stable cell-cell contacts, it still seemed possible that different aspects of synapse formation, for example receptor recruitment and MTOC reorientation, might require MyH9 motor activity. Thus, we investigated whether cells could productively reorient membrane receptors and cytoskeletal components in the presence of blebbistatin. For these experiments, we pretreated day 6 T cell blasts with 50 μM blebbistatin or vehicle control for 30 min and then briefly spun together the T cells and ovalbumin (OVA) peptide–pulsed B cells to bypass the crawling defect of blebbistatin-treated T cells. After 30 min of incubation at 37 °C, the cells were fixed and stained with specific antibodies and analyzed by fluorescence microscopy. Immunological synapse recruitment was normal with respect to CD3 and LFA-1 relocalization in T cell–B cell conjugates formed in the absence of MyH9 function (**Fig. 6a** and **Supplementary Fig. 3**). In addition, actin assembly at the synapse was unaffected, because actin adhesion rings were found in T cell–B cell conjugates formed with blebbistatin- or DMSO-treated T cells, and MTOC reorientation occurred normally in the presence of MyH9 blockade. Finally, MyH9 still accumulated at the synapse even in the presence of blebbistatin, indicating that this accumulation may be the result of a passive mechanism or that another motor protein may be responsible for MyH9 recruitment to T cell–APC interface (**Fig. 6a** and **Supplementary Fig. 3**). We also analyzed the formation of central supra-molecular activation clusters (c-SMACs) of TCRs and peripheral-SMACs of LFA-1 by three-dimensional T cell–APC interface reconstruction in cells treated with blebbistatin or with DMSO. Although in our experimental system the overall frequency of prototypical SMAC distributions was low, we found no relevant differences between control (32.1% CD3-LFA-1 SMACs, $n = 28$) and blebbistatin-treated cells (28.6% CD3-LFA-1 SMACs, $n = 28$) (**Fig. 6b**).

TCR-induced phosphorylation of MyH9

Although our data showed that MyH9 is not necessary for immunological synapse formation, its key role in motility implies that it might be important for T cells to deactivate this myosin to permit the transition between crawling and T cell–APC conjugate formation. In rat mast cells, calcium-dependent phosphorylation of the MyH9 C-terminal residues Ser1917 and Thr1940 (equivalent to mouse Ser1916 and Thr1939, respectively) has been proposed to contribute to cytoskeletal rearrangements, facilitating access of secretory granules to the plasma membrane[27,28]. Because TCR stimulation generates the stop signal and induces the morphological transition in T cells[5,9], we assessed the phosphorylation state of the MyH9 heavy chain during TCR stimulation. Encounter of T cell blasts with antigen-pulsed APCs induced phosphorylation of MyH9 at Thr1939 in the C-terminal region of the myosin tail (**Fig. 7a**). To further assess whether TCR stimulation induced this phosphorylation in the absence of accessory signals, we stimulated T cell blasts with anti-CD3. Phosphorylation of Thr1939 of MyH9 in T cells peaked after 2 min of TCR stimulation, returning to baseline after 20 min (**Fig. 7b**). We also analyzed the phosphorylation status of Ser1916 of MyH9 and Ser19 and Thr20 of the myosin light chains but did not detect any antigen-induced changes (data not shown).

Because increased cytosolic calcium is an important second messenger in T cell activation, underlies the stop signal and is implicated in MyH9 phosphorylation in mast cells, we assessed the requirement for calcium signaling and the ability of the calcium ionophore ionomycin, phorbol myristate acetate (PMA) or both to induce MyH9 phosphorylation in T cells. Intracellular calcium transients were necessary and sufficient to induce threonine phosphorylation of MyH9 (**Fig. 7c**,**d**). Thus, the antigen-induced phosphorylation of MyH9 Thr1939 showed a direct connection between TCR signals and myosin motors, suggesting a role for MyH9 as a part of the T cell stop signal.

DISCUSSION

According to the general model of class II myosin function in migrating cells, actin polymerization generates lamellipodial membrane protrusions at the leading edge of cells, which serve as anchors to the substratum. Subsequently, myosin-dependent forces pull or push the cellular body forward while cells detach their trailing edge by regulating integrin adhesiveness[29,30]. Two principal mechanisms for myosin-generated traction force have been proposed. According to the 'contraction' model, cells form stronger

adhesion contacts at their leading edge as compared to their trailing edge and actin contraction induced by myosin activity results in a net forward movement of the cell. In the 'transport' model, polarized actin filaments serve as tracks for directed movement generated by class II myosin motors[30,31]. Further variations in the mechanisms of myosin based crawling are dependent on cell type, based on differences in cytoskeletal structure, morphology and speed of the cells during migration.

For T cells, the exact mechanism by which class II myosins promote polarity and migration has not yet been fully addressed. The high speed at which T cells migrate, as compared to fibroblasts and endothelial cells, and the fact that they do not form stress fibers or focal adhesions are suggestive of a continuous and coordinated remodeling of the actomyosin cytoskeleton[8]. On the basis of two lines of indirect evidence obtained here, it is more likely that migration of T cells may occur through an extrusive process based in the uropod.

First, MyH9 was enriched at the uropod, particularly at the head-tail junction, indicating that this is its primary site of action during crawling. Such data are consistent with the posterior localization of myosin II during chemotaxis in *D. discoideum*[32]. In addition, in response to nondirectional stimuli, myosin II in *D. discoideum* is cortically distributed and is accompanied by the absence of a uropodal projection[33]. We have also observed small, submembrane, MyH9 packet–like structures that migrate rearward from pseudopodal projections and the head-tail junction. This either might suggest that MyH9 aids crawling by retracting membrane away from pseudopodia and into a highly tensioned uropodal structure or, alternatively, might represent static accumulations of MyH9 on a mobile cytoskeletal structure. The velocity of the motile intracellular packets (0.21 ± 0.04 μm/s) was similar to the previously established *in vitro* motility speed of MyH9 (0.29 ± 0.03 μm/s), consistent with their propulsion by MyH9 itself[34]. That these packets move backward at a pace that is faster than the cell projects forward supports a model whereby MyH9 retracts excess membrane into the uropod. Further, the relative paucity of MyH9 at the leading edge makes it less likely that the motor acts from this location.

Second, specific inhibition of class II myosin indicated that T cells require MyH9 motor activity to maintain their characteristic hand-mirror morphology and that in the absence of MyH9 function T cells are unable to crawl. Our data also showed that this motor is necessary for cellular translocation but that the leading-edge activities that use the actin cytoskeleton may not require myosin function and might depend only on actin polymerization.

An appealing model for the role of the T cell uropod is that it may serve as the main site of contraction for the actin cytoskeleton, generating the extrusive force needed to propel the bulk of the cytoplasm forward into the leading edge. In this regard, the role of myosin II in closing the cleavage furrow during cytokinesis and pinching off daughter cells in *D. discoideum* may represent a similar constrictive function of myosin II.

MyH9 has been found in association with the chemokine receptor CXCR4 in T cells in cell lysates[35]. Although this interaction has intriguing implications for chemotactic polarity, more work is required to determine whether chemokine receptors can recruit MyH9 to the leading edge where they are typically localized[7]. Alternatively, chemokine receptors might associate with and deactivate MyH9 at the leading edge, rather than activating MyH9 for propulsive purposes in the uropod.

An important result of our study is that MyH9 may be a regulatory site for TCR-induced effects on the cytoskeleton. Notably, the residue phosphorylated on activation of T cells, Thr1939, is in the C-terminal domain of MyH9, directly adjacent to the coiled-coil domain. Evidence from *D. discoideum* demonstrates that the activities of myosin II require the motors to be in the form of thick filaments. In this system, as in many others, threonine or serine phosphorylation of the tail portion of the heavy chain, catalyzed by protein kinase C, calmodulin (CaM) kinase and the casein-kinase families, destabilizes the coiled-coil interactions that maintain filament assembly. Phosphorylation induces the dissociation of myosin II bipolar filaments, which releases cellular cortical tension provided by the actin cytoskeleton[22,36,37]. Although evidence for a similar mechanism of regulation of MyH9 in mammalian cells is not clear, phosphorylation of Thr1939 could also affect filament formation in less direct ways, for example by modulating the interaction of other proteins with MyH9. Mts-1, a member of the S100 family of calcium-binding proteins that is upregulated in active motile cells and in cancer cells, has been proposed as one such player[38,39]. Mts-1 binds to the tail of MyH9 between residues 1909 and 1937, inducing partial filament depolymerization[40]. Phosphorylation of Thr1939 may thus modulate binding to Mts-1 as a means of regulating filament formation.

In contrast to such signals, light chain activation of myosins frequently occurs through the CaM–myosin light chain kinase (MLCKs) pathway, which, in turn, is activated by calcium influxes. This calcium-dependent phosphorylation of the regulatory light chains by MLCKs, Rho kinase or p21-activated kinase causes activation of myosin II by increasing ATPase and motor activities[22,41,42]. MyH9 phosphorylation resulting in downregulation of motor function may explain how T cells undergoing TCR signaling can cease crawling despite high calcium concentrations that would other wise be expected to induce the activity of calcium-dependent proteins.

Our results provide evidence against a direct role for myosin II in synapse formation in T cells. This result was somewhat unexpected, as previous work has implicated myosin motors in reversing the retrograde membrane flow in T cells and transporting key surface molecules, including CD3, into the immunological synapse[14]. This study did not, however, identify the specific myosins involved in the process, owing to the relative lack of selectivity of the general myosin inhibitor (butanedione monoxime) used[14]. Therefore, as our data imply that MyH9 is not required for assembly of the immunological synapse, the active transport of membrane components and receptors to the T cell–APC interface must rely on some other (non–class II) motor proteins, most likely unconventional myosins.

The release of uropodal tension and cessation of crawling is nevertheless an integral step in initiating synapse formation. Our findings indicate that MyH9 motor activity, though required for migration and polarization, may be inactivated as part of the stop signal. The TCR and calcium dependence of heavy chain phosphorylation parallels the TCR and calcium dependence of cell arrest and rounding that have been observed previously[5,9]. Although phosphorylation cannot immediately be detected after TCR stimulation using our methods, cessation of motility and dissolution of the uropod also lags at least 30 s behind calcium influx[5]. To this extent, synapse formation and long-term signaling may rely intricately on the regulation of this motor, as disregulation would be expected to prevent long-term APC contacts from being established. Taken together, the requirement for MyH9 function in T cell crawling, the ability to form synapses in the absence of MyH9 activity and the TCR-induced phosphorylation of this myosin indicate that MyH9 regulation may be one of the mechanisms controlling the T cell stop signal.

METHODS

Cells and mice. Naive and activated T cells were derived from DO11.10 TCR transgenic mice (in a BALB/c background) purchased from Jackson Laboratories. The transgenic TCR expressed by DO11.10 T cells recognizes the OVA(323–339) peptide in the context of MHC class II I-A^d (ref. 43). The D10.G4-IL2 $CD4^+$ T cell clone derived from AKR/J mice was maintained in RPMI medium supplemented with 50 U/ml interleukin-2 (IL-2). This T cell clone recognizes the conalbumin(134–146) peptide in the context of MHC class II IA^k (ref. 44). A20 and CH27 B cell lines were used as APCs for I-A^d and I-A^k MHC class II peptide presentation, respectively. All mice were bred and maintained in accordance with the guidelines of the Lab Animal Resource Center of the University of California at San Francisco.

Antibodies and reagents. The following primary antibodies were used for cell staining, immunoblotting or T cell stimulation: rabbit anti–class II myosin polyclonal (BTI); rabbit isoform-specific anti-MyH9 and anti-MyH10 (Covance); rabbit anti-MyH14 (a kind gift of R.S. Adelstein[34]); hamster anti-CD3 500.A2 and rat anti-LFA-1 M17/4 (both from Pharmingen); and biotinylated anti-tubulin (Molecular Probes).

A rabbit polyclonal antibody was raised against a phosphopeptide corresponding to amino acids RIVRKGTGDCSDE of the mouse MyH9 heavy chain (anti-pThr1939-MyH9). The antibody was affinity purified using the phosphopeptide and then cross-adsorbed with nonphosphorylated peptide to give a phospho-specific antibody. Lysates from carbachol-stimulated and unstimulated rat basophilic leukemia cells, RBL-2H3 (ref. 28), were used to confirm specificity for pThr1939 of MyH9 (**Supplementary Fig. 4**). In addition, MyH9 was immunoprecipitated from lysates of unstimulated or CD3-stimulated DO.11.10 T cells; the MyH9 immunoprecipitates were then immunoblotted with anti-pThr1939-MyH9 as a further specificity control (**Supplementary Fig. 4**).

Unconjugated and rhodamine-conjugated goat anti-hamster, FITC-conjugated donkey anti-rat, FITC- and rhodamine-conjugated donkey anti-rabbit and FITC-conjugated streptavidin secondary reagents were purchased from Jackson ImmunoResearch Laboratories. Rhodamine-phalloidin, CFSE fluorescent cellular dye and Fura2-AM ester ratiometric calcium dye were from Molecular Probes. PKH26 red fluorescent membrane dye, aprotinin, leupeptin, phenylmethylsulfonyl fluoride (PMSF), sodium fluoride, iodoacetamide and sodium orthovanadate were purchased from Sigma. Horseradish peroxidase–conjugated goat anti-mouse and protein A, and detergent-compatible protein assay kit, were purchased from Bio-Rad. Blebbistatin was purchased from Calbiochem and was used at 50 μM with a 30-min pretreatment and kept present during the various assays. Because this drug is light sensitive, its activity in each experiment was verified by the observation of rounded cells lacking uropods.

Cell stimulation, lysis and immunoblotting. For antibody stimulations, DO11.10 day 6 T cell blasts were starved in serum-free RPMI for 1 h, incubated with saturating doses of anti-CD3 for 30 min at 4 °C, washed and then stimulated for different lengths of time at 37 °C with soluble goat anti-hamster secondary antibody. In T cell stimulation experiments, we used 500 ng/ml ionomycin, 10 ng/ml PMA and 5 mM EDTA. For T cell stimulation through B cell coupling, DO11.10 day 6 T cell blasts were starved of serum and then mixed 2:1 with either A20 B cells pulsed with 1 μg/ml OVA(323–339) or unpulsed controls, and incubated for different times at 37 °C. Cells were lysed in modified RIPA lysis buffer (150 mM NaCl, 1 mM $CaCl_2$, 1 mM $MgCl_2$ and 1% Triton X-100 in PBS) containing a cocktail of protease and phosphatase inhibitors (2 μg/ml aprotinin, 2 μg/ml leupeptin, 2 mM PMSF, 10 mM sodium fluoride, 10 mM iodoacetamide and 1 mM sodium orthovanadate). Aliquots of cell lysates containing equal amounts of protein, as determined with the Bio-Rad detergent-compatible protein assay, were resolved by SDS-PAGE. This was followed by immunoblotting analysis with anti-pThr1939-MyH9 and then by stripping and reblotting with an anti-MyH9 (Covance).

siRNA vector construction and transfection. The siRNA constructs were constructed using the U6 tRNA promoter driving expression of a short siRNA sequence specific for the MyH9 gene (5′-GGGTGCCTTCCAGCAAGAATGG-3′) or a control nonsilencing sequence (5′-AATTCTCCGAACGTGTCACGT-3′). These PCR generated constructs were inserted into the pGEM-T easy cloning vector (Promega). Anti-MyH9 or control siRNA plasmids were then electroporated into D10 T cells along with a GFP-expressing plasmid at a 10:1 ratio. At 24 or 48 h after transfection, GFP-positive cells were sorted and used for experiments.

Microscopy. Imaging experiments were done using a modified Zeiss Axiovert 200M microscope with a plan-neofluar ×40 objective (Carl Zeiss). The microscope was fitted with dual excitation and emission filter wheels and a Photometrics Coolsnap-HQ camera. The imaging and control software used was Metamorph (Universal Imaging). For morphology and crawling experiments, 10^5 untransfected or MyH9-GFP-transfected D10 T cells were plated into coverslip wells (Nunc) and kept at 37 °C on the heated stage of the microscope. Data collection of differential interference contrast (DIC) and green fluorescence (for transfected cells) images was done at 5-s intervals over a period of 30 min. For live coupling assays, D10 T cells were loaded with 1 μM Fura2-AM for 20 min at room temperature (22–25 °C), washed and plated onto coverslips on the heated stage. Antigen-pulsed CH27 APCs (1 μg/ml conalbumin(134–146) peptide) were then added and imaging was carried out at 30-s intervals for 30 min. Calcium concentrations were measured using the calcium-sensitive ratiometric dye Fura2-AM and are shown in a pseudo color scale (range: blue-green-yellow-red-white) reflecting increases in the intracellular calcium concentration. We collected DIC, Fura2 340-nm emission, Fura2 380-nm emission and green fluorescence images for each time point.

Fixed cell staining was done by briefly spinning together 10^5 day 6 DO11.10 T cell blasts (treated with DMSO or blebbistatin) with an equal number of A20 B cells pulsed with 1 μg/ml OVA peptide as APCs. The cells were incubated at 37 °C for 30 min and then fixed with 1% paraformaldehyde at room temperature for 15 min. Fixed cell samples were antibody stained by spotting cells on slides, blocking with 3% goat or donkey serum and permeabilizing with 0.02% saponin in PBS for 30 min. The primary antibodies were incubated for 60 min, then extensively washed and subjected to secondary antibody staining for 60 min. After thorough washing, the cells were treated with anti-fade reagent (Bio-Rad) and the slides were sealed and imaged. CD3-LFA-1 SMAC distribution experiments were carried out on D10 T cell clones with CH27 as APCs using the same conditions described above.

Molecule redistribution in T cell–APC conjugates was scored using the following criteria: if fluorescence intensity at the synapse was at least 1.5 times the average intensity level of the rest of the cell and no other major high-intensity 'spots' were present, the couple was scored as fully polarized; if additional high-intensity spots were present at sites other than the T cell–APC interface, the couple was scored as partially polarized; and if the intensity at the synapse was below the set threshold, the couple was scored as negative. All image analysis and measurements were done using Metamorph software.

Coupling assay. D10 T cells were loaded with 5 μM CFSE at 37 °C for 15 min and then washed. Conalbumin-pulsed CH27 B cells were labeled with 2 μM of the red fluorescent dye PKH26 at RT for 10 min and then washed according to the manufacturer's protocol. 10^5 T cells and B cells were mixed together and incubated at 37 °C for 45 min, with or without an initial centrifugation step of 1 min at 300*g*. After incubation, the cells were immediately analyzed on a FACSCalibur cytofluorimeter (Becton Dickinson) to quantify the percentage of conjugate formation. This percentage was quantified as the number of double-positive T cells (CFSE- and PKH26-positive) versus total numbers of T cells (CFSE-positive).

Morphology quantitation and packet tracking. D10 T cells were seeded into glass coverslips, allowed to re-adhere and then treated for 30 min with blebbistatin (50 μM) or DMSO. DIC images of the cells were then acquired. Uropodal morphology was scored either visually (analyzing 50 cells per treatment condition) or by measuring the elliptical form factor—cell length divided by its breadth, with a score of 1 equaling to a round cell—of the cells (analyzing 20 cells per condition). The uropodal morphology of T cells was also assessed after MyH9-specific siRNA transfection (described above). A minimum of 36 GFP-positive cells were scored visually for both the specific and control siRNA.

The speed of MyH9-GFP packets was measured with the 'track point' function of Metamorph on time-lapse videos of transfected crawling T cells. Eight

packets were randomly selected from five crawling cells; their normalized velocities were measured relative to cell body velocity and these were averaged over the duration of the packet's movement.

Note: Supplementary information is available on the Nature Immunology website.

ACKNOWLEDGMENTS

We thank A. Weiss and S. Reck-Peterson (University of California at San Francisco) for comments on the manuscript, R.S. Adelstein (National Heart, Lung and Blood Institute, National Institutes of Health) for kindly providing us with the human MyH9-GFP fusion construct and for the MyH14 specific antibody, and S. Jiang for expert technical assistance with cell sorting. J.J. was supported in part by a fellowship from the Fondazione Italiana per la Ricerca sul Cancro. This work was supported by a grant from the US National Institutes of Health (RO1-AI52116-01) and from the Howard Hughes Medical Institute Biomedical Research Support Program (#5300246).

COMPETING INTERESTS STATEMENT

The authors declare that they have no competing financial interests.

Received 9 December 2003; accepted 1 March 2004
Published online at http://www.nature.com/natureimmunology/

1. Sanchez-Madrid, F. & del Pozo, M.A. Leukocyte polarization in cell migration and immune interactions. *EMBO J.* **18**, 501–511 (1999).
2. Miller, M.J., Wei, S.H., Parker, I. & Cahalan, M.D. Two-photon imaging of lymphocyte motility and antigen response in intact lymph node. *Science* **296**, 1869–1873 (2002).
3. Bousso, P. & Robey, E. Dynamics of CD8+ T cell priming by dendritic cells in intact lymph nodes. *Nat. Immunol.* **4**, 579–585 (2003).
4. McFarland, W. & Heilman, D.H. Lymphocyte foot appendage: its role in lymphocyte function and in immunological reactions. *Nature* **205**, 887–888 (1965).
5. Negulescu, P.A., Krasieva, T.B., Khan, A., Kerschbaum, H.H. & Cahalan, M.D. Polarity of T cell shape, motility, and sensitivity to antigen. *Immunity* **4**, 421–430 (1996).
6. Donnadieu, E., Bismuth, G. & Trautmann, A. Antigen recognition by helper T cells elicits a sequence of distinct changes of their shape and intracellular calcium. *Curr. Biol.* **4**, 584–595 (1994).
7. Nieto, M. *et al.* Polarization of chemokine receptors to the leading edge during lymphocyte chemotaxis. *J. Exp. Med.* **186**, 153–158 (1997).
8. Vicente-Manzanares, M., Sancho, D., Yanez-Mo, M. & Sanchez-Madrid, F. The leukocyte cytoskeleton in cell migration and immune interactions. *Int. Rev. Cytol.* **216**, 233–289 (2002).
9. Dustin, M.L., Bromley, S.K., Kan, Z., Peterson, D.A. & Unanue, E.R. Antigen receptor engagement delivers a stop signal to migrating T lymphocytes. *Proc. Natl Acad. Sci. USA* **94**, 3909–3913 (1997).
10. Krummel, M.F., Sjaastad, M.D., Wülfing, C. & Davis, M.M. Differential assembly of CD3z and CD4 during T cell activation. *Science* **289**, 1349–1352 (2000).
11. Monks, C.R.F., Freiberg, B.A., Kupfer, H., Sciaky, N. & Kupfer, A. Three-dimensional segregation of supramolecular activation clusters in T cells. *Nature* **395**, 82–86 (1998).
12. Grakoui, A. *et al.* The immunological synapse: A molecular machine that controls T cell activation. *Science* **285**, 221–226 (1999).
13. Kupfer, A. & Singer, S.J. The specific interaction of helper T cells and antigen-presenting B cells: IV. Membrane and cytoskeletal reorganizations in the bound T cell as a function of antigen dose. *J. Exp. Med.* **170**, 1697–1713 (1989).
14. Wülfing, C. & Davis, M.M. A receptor/cytoskeletal movement triggered by costimulation during T cell activation. *Science* **282**, 2266–2269 (1998).
15. Wulfing, C., Sjaastad, M.D. & Davis, M.M. Visualizing the dynamics of T cell activation: intracellular adhesion molecule 1 migrates rapidly to the T cell/B cell interface and acts to sustain calcium levels. *Proc. Natl Acad. Sci. USA* **95**, 6302–6307 (1998).
16. Villalba, M. *et al.* Vav1/Rac-dependent actin cytoskeleton reorganization is required for lipid raft clustering in T cells. *J. Cell Biol.* **155**, 331–338 (2001).
17. Moss, W.C., Irvine, D.J., Davis, M.M. & Krummel, M.F. Quantifying signaling-induced reorientation of T cell receptors during immunological synapse formation. *Proc. Natl. Acad. Sci. USA* **99**, 15024–15029 (2002).
18. Mermall, V., Post, P.L. & Mooseker, M.S. Unconventional myosins in cell movement, membrane traffic, and signal transduction. *Science* **279**, 527–533 (1998).
19. Sellers, J.R. Myosins: a diverse superfamily. *Biochim. Biophys. Acta* **1496**, 3–22 (2000).
20. Berg, J.S., Powell, B.C. & Cheney, R.E. A millennial myosin census. *Mol. Biol. Cell* **12**, 780–794 (2001).
21. Leal, A. *et al.* A novel myosin heavy chain gene in human chromosome 19q13.3. *Gene* **312**, 165–171 (2003).
22. Bresnick, A.R. Molecular mechanisms of nonmuscle myosin-II regulation. *Curr. Opin. Cell Biol.* **11**, 26–33 (1999).
23. Straight, A.F. *et al.* Dissecting temporal and spatial control of cytokinesis with a myosin II Inhibitor. *Science* **299**, 1743–1747 (2003).
24. De Lozanne, A. & Spudich, J.A. Disruption of the *Dictyostelium* myosin heavy chain gene by homologous recombination. *Science* **236**, 1086–1091 (1987).
25. Doolittle, K.W., Reddy, I. & McNally, J.G. 3D analysis of cell movement during normal and myosin-II-null cell morphogenesis in dictyostelium. *Dev. Biol.* **167**, 118–129 (1995).
26. Wei, Q. & Adelstein, R.S. Conditional expression of a truncated fragment of nonmuscle myosin II-A alters cell shape but not cytokinesis in HeLa cells. *Mol. Biol. Cell* **11**, 3617–3627 (2000).
27. Ludowyke, R.I., Peleg, I., Beaven, M.A. & Adelstein, R.S. Antigen-induced secretion of histamine and the phosphorylation of myosin by protein kinase C in rat basophilic leukemia cells. *J. Biol. Chem.* **264**, 12492–12501 (1989).
28. Buxton, D.B. & Adelstein, R.S. Calcium-dependent threonine phosphorylation of nonmuscle myosin in stimulated RBL-2H3 mast cells. *J. Biol. Chem.* **275**, 34772–34779 (2000).
29. Lauffenburger, D.A. & Horwitz, A.F. Cell migration: a physically integrated molecular process. *Cell* **84**, 359–369 (1996).
30. Mitchison, T.J. & Cramer, L.P. Actin-based cell motility and cell locomotion. *Cell* **84**, 371–379 (1996).
31. Heidemann, S.R. & Buxbaum, R.E. Cell crawling: first the motor, now the transmission. *J. Cell Biol.* **141**, 1–4 (1998).
32. Liang, W., Licate, L., Warrick, H., Spudich, J. & Egelhoff, T. Differential localization in cells of myosin II heavy chain kinases during cytokinesis and polarized migration. *BMC Cell Biol.* **3**, 19 (2002).
33. Levi, S., Polyakov, M.V. & Egelhoff, T.T. Myosin II dynamics in *Dictyostelium*: determinants for filament assembly and translocation to the cell cortex during chemoattractant responses. *Cell Motil. Cytoskeleton* **53**, 177–188 (2002).
34. Golomb, E. *et al.* Identification and characterization of nonmuscle myosin II–C, a new member of the myosin II family. *J. Biol. Chem.* **279**, 2800–2808 (2004).
35. Rey, M. *et al.* Cutting edge: association of the motor protein nonmuscle myosin heavy chain-IIA with the C terminus of the chemokine receptor CXCR4 in T lymphocytes. *J. Immunol.* **169**, 5410–5414 (2002).
36. Egelhoff, T.T., Lee, R.J. & Spudich, J.A. *Dictyostelium* myosin heavy chain phosphorylation sites regulate myosin filament assembly and localization *in vivo*. *Cell* **75**, 363–371 (1993).
37. Redowicz, M.J. Regulation of nonmuscle myosins by heavy chain phosphorylation. *J. Muscle Res. Cell Motil.* **22**, 163–173 (2001).
38. Ebralidze, A. *et al.* Isolation and characterization of a gene specifically expressed in different metastatic cells and whose deduced gene product has a high degree of homology to a Ca^{2+}-binding protein family. *Genes Dev.* **3**, 1086–1093 (1989).
39. Ford, H.L., Salim, M.M., Chakravarty, R., Aluiddin, V. & Zain, S.B. Expression of *Mts1*, a metastasis-associated gene, increases motility but not invasion of a nonmetastatic mouse mammary adenocarcinoma cell line. *Oncogene* **11**, 2067–2075 (1995).
40. Ford, H.L., Silver, D.L., Kachar, B., Sellers, J.R. & Zain, S.B. Effect of Mts1 on the structure and activity of nonmuscle myosin II. *Biochemistry* **36**, 16321–16327 (1997).
41. Kamm, K.E. & Stull, J.T. Dedicated myosin light chain kinases with diverse cellular functions. *J. Biol. Chem.* **276**, 4527–4530 (2001).
42. Amano, M. *et al.* Phosphorylation and activation of myosin by Rho-associated kinase (Rho-kinase). *J. Biol. Chem.* **271**, 20246–20249 (1996).
43. Murphy, K.M., Heimberger, A.B. & Loh, D.Y. Induction by antigen of intrathymic apoptosis of $CD4^+CD8^+TCR^{lo}$ thymocytes *in vivo*. *Science* **250**, 1720–1723 (1990).
44. Kaye, J., Porcelli, S., Tite, J., Jones, B. & Janeway, C.A., Jr. Both a monoclonal antibody and antisera specific for determinants unique to individual cloned helper T cell lines can substitute for antigen and antigen-presenting cells in the activation of T cells. *J. Exp. Med.* **158**, 836–856 (1983).